Simulation and Analysis of Magnetisation Characteristics of Interior Permanent Magnet Motors

J. A. Walker, C. Cossar, T. J. E. Miller

Modern permanent magnet (PM) synchronous brushless machines often have magnetic circuits in which the patterns of saturation are complex and highly variable with the position of the rotor. The classical phasor diagram theory of operation relies on the assumption of sinusoidal variation of flux-linkage with rotor position, and neglects the non-linear effects that arise in different operating states. The finite element method is a useful tool for detailed magnetic analysis, but it is important to verify simulation results by direct measurement of the magnetic characteristics of the motor, in terms of "magnetisation curves" of current and flux-linkage. This paper presents results from finite element simulations to determine the magnetisation in a split-phase interior permanent magnet (IPM) motor. Investigation has been made to determine the effects of the rotor geometry on the synchronous reactances and airgap flux distribution. Comparisons are made with a second IPM motor with a different rotor configuration.

Keywords: permanent magnet, finite element method, flux-linkage measurement, rotor bridges.

Notation and units

E	voltage associated with the permanent magnets	[V]
E_0	open circuit magnet voltage	[V]
Ψ_1	fundamental flux-linkage associated with B_1	[V-s]
B_1	peak value of fundamental airgap flux density	[T]
D	bore diameter	[m]
L_{stk}	stack length	[m]
N_{ph}	number of phases	
k_{w1}	fundamental winding factor	
p	number of pole pairs	
X_q	quadrature axis synchronous reactance	[Ω]
X_d	direct axis synchronous reactance	[Ω]
R	phase resistance	[Ω]
ω	angular frequency	[rad/sec]
I	phase current	[A]
i	instantaneous current	[A]
I_q	quadrature axis current component	[A]
I_d	direct axis current component	[A]
$R_{A,B}$	non-inductive resistance	[Ω]
R_{VAR}	variable resistance	[Ω]
R_M	winding resistance	[Ω]
L_M	winding inductance	[H]
Ψ	flux-linkage due to current from Wheatstone bridge	[V-s]

1 Introduction

The permanent magnet synchronous motor (PMSM) has risen in prominence owing to its comparably high efficiency and torque per volume ratio. The motor is salient-pole and highly saturable. The rotor may have interior rather than surface-mounted magnets, and may include a cage for starting. The saturation of the magnetic circuit varies with rotor position, resulting in localised effects. The operation of the motor can be analysed using the phasor diagram method, which transforms the phase currents and flux-linkages into direct (polar) and quadrature (interpolar) axis components. The direct axis (d-axis) flux-linkage can be split into two contributions, one from the current and one from the permanent magnets. The EMF associated with the magnets is denoted by the resultant EMF, E. There is no flux-linkage contribution from the permanent magnets on the quadrature axis (q-axis). It is not possible to measure the EMF associated with the magnets with current flowing in the winding and so it is necessary to assume that it remains constant at the open circuit value E_0, irrespective of loading.

As the diagram is based on phasor quantities, it can only be used to calculate sine-wound motors driven by sinusoidal voltages and currents. In cases where the winding distribution is non-sinusoidal, or where the excitation waveforms are non-sinusoidal, it is useful to analyse the motor using Finite Element (FE) software. It is not possible to separate the total flux-linkage calculated using finite elements without resorting to superposition, which cannot be considered valid in the case of non-linear magnetic circuits. Regardless of the method used, it is important to verify the results by measurement. The amount of magnet flux crossing the airgap is heavily dependent on the rotor design. The rotor slots are sometimes fully enclosed by bridge sections, which lowers the noise or harmonic content in the airgap flux distribution. The bridges quickly saturate and create magnetic short circuits within the rotor, contributing significantly to the levels of leakage flux and thus reducing the amount of flux crossing the airgap. The rotor slots can be designed so as to provide lower harmonic content in the flux density whilst limiting leakage flux.

2 Simulation of magnetic characteristics using finite elements

The motor cross sections can be modelled by finite elements, as shown in Fig. 1 [1]. Single load point simulations can be run to determine the airgap flux density distribution

when the phase axis is aligned with the direct and quadrature axis rotor positions, for increasing load current. The direct and quadrature axis synchronous reactances are calculated from the fundamental component of the airgap flux density. The peak fundamental flux-linkage is given by (1) and then the RMS synchronous reactances can be calculated from (2) and (3).

$$\Psi_1 = \frac{B_1 D L_{\text{stk}} N_{\text{ph}} k_{\text{w1}}}{p} \quad \text{[V-s]} \quad (1)$$

$$X_{\text{d}} = \frac{\frac{\Psi_1 \omega}{\sqrt{2}} - E_0}{I} \quad [\Omega] \quad (2)$$

$$X_{\text{q}} = \frac{\Psi_1 \omega}{I\sqrt{2}} \quad [\Omega] \quad (3)$$

According to (2), the direct axis synchronous reactance calculation requires separation of the current component of flux-linkage from the magnet component. It is, therefore, once again convenient to assume that the open circuit magnet flux is constant and independent of loading. The properties of the permanent magnets can be matched in the finite element simulations by comparing simulated open circuit back EMF waveforms to experimental results.

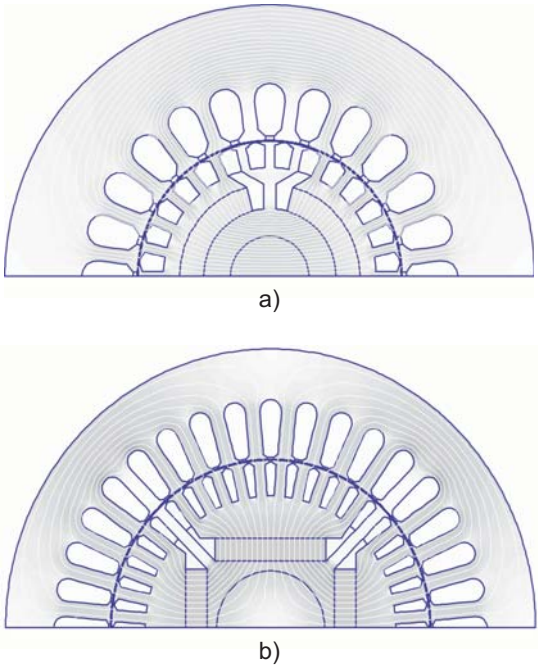

Fig. 1: Finite element plots a) Test Motor 1, b) Test Motor 2

The static magnetisation curves of the motor represent the variation of flux-linkage with current at successive rotor positions and can be represented in terms of either the direct and quadrature axes or phase quantities. By minor alteration of a scripting routine in the finite element software, it is possible to calculate the flux-linkages at incremental rotor positions with constant current in the winding. The flux-linkage is calculated from the magnetic vector potential in each of the stator slots and so the direct axis value includes the flux-linkage contributions from both the direct axis current and the permanent magnets.

3 Verification of simulation results by measurement

The testing of IPM motors necessarily differs from that of wound-field synchronous machines, due to the permanent excitation resulting from the magnets. For wound-field machines, the synchronous reactances are measured from open circuit saturation tests and short-circuit tests in accordance with IEEE Standard 115-1995 [2]. The method for determining synchronous reactances, independently discovered by Jones and El-Kharashi [3, 4], was first applied to permanent magnet motors by Miller [7]. The phase of the motor to be tested is connected into one leg of a Wheatstone bridge circuit, as in Fig. 2. The resistance R_{M} and inductance L_{M} represent the winding under test. The variable resistor R_{VAR} is adjusted so that when the switch is open there is no voltage across the centre of the bridge. The switch is initially closed, to allow a DC current I_{DC} to flow through the bridge circuit. When the switch is then opened, the current through the inductor decays from I_{DC} to zero. During this transient period, the voltage across the centre of the bridge is given by (4). The voltage waveform is stored in a digital storage oscilloscope (DSO). By integrating this voltage with respect to time, the flux-linkage for the given level of current can be found. If the bridge is balanced and the resistor ratios have been selected such that $R_{\text{A}} = R_{\text{B}}$, then the inductance of the winding is given by (5). From this, the synchronous reactances can be determined (6). The synchronous reactances will vary as a function of load.

$$v = v_{R_{\text{B}}} - v_{R_{\text{VAR}}} = -\frac{R_{\text{VAR}}}{R_{\text{VAR}} - R_{\text{M}}} L_{\text{M}} \frac{\text{d}i}{\text{d}t} \quad \text{[V]} \quad (4)$$

$$L_{\text{M}} = \frac{2\Psi}{I_{\text{DC}}} \quad \text{[H]} \quad (5)$$

$$X = \omega L_{\text{M}} \quad [\Omega] \quad (6)$$

The direct measurement of magnetisation curves in switched reluctance motors using locked rotor tests with pulsed voltage waveforms is described by Miller, [5]. The bridge circuit used for measurement of the synchronous reactances can be incorporated into the locked rotor test rig. However, the flux-linkage calculated by integration of the instantaneous voltage is due to winding current only and does not include any contribution from the permanent magnets. It is commonly assumed that the flux-linkage contribution from the permanent magnets is independent of current and varies only with rotor position. Under this assumption, the contribu-

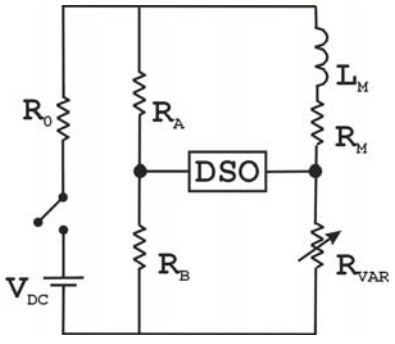

Fig. 2: Wheatstone bridge circuit for measurement of synchronous reactances

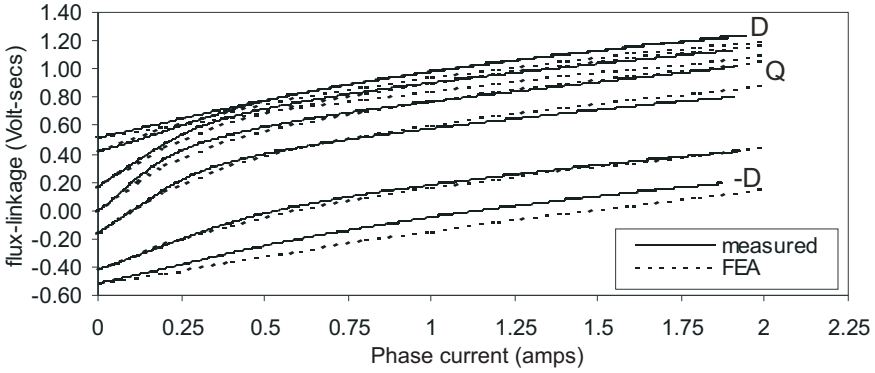

Fig. 3: Comparison between measured and FE-simulated magnetisation curves

tion from the magnets can be calculated from integration of the open circuit back EMF waveform. An indirect method of verifying the magnet flux-linkage with current in the winding, combining the Wheatstone bridge circuit and a rotational test, has been discussed by Miller et al. [6]. The rotor is locked into position and the flux-linkage due to current measured as for the synchronous reactance measurements. The rotor is then rotated through a predetermined angle and the change in flux-linkage added to the flux-linkage from the Wheatstone bridge measurement. The result will be the total flux-linkage at the new rotor position. The flux-linkage due to current at the new rotor position is easily measured using the bridge circuit. Subtraction of this value from the total flux-linkage leaves the magnet flux-linkage contribution at the new rotor position, which if the magnet flux is independent of current, will equal the open circuit magnet flux-linkage at that rotor angle.

Taking the starting point for the measurements as the quadrature axis, there will be no flux-linkage contribution from the permanent magnets and so the q-axis magnetisation curve can be determined solely from the Wheatstone bridge circuit. Using the rotational test method, the total flux-linkage at each successive rotor position will be the sum of the flux-linkage at the previous rotor position and the change in flux-linkage measured during rotation. In this way, the complete set of magnetisation curves can be measured without any assumption of the magnet flux-linkage. Measured magnetisation curves for test motor 1 have been compared with simulated results, shown as dashed lines, in Fig. 3.

4 Analysis of magnetisation characteristics

Simulations have been run on two test motors. Parameter information is given in Appendix 1. Simulation results from the first test motor have been compared with measured values for verification. The flux-linkages due to current of motor 1, a split-phase, 2 pole IPM motor are shown in Fig. 4. The quadrature axis synchronous reactance is higher than that of the direct axis, due to presaturation of the direct axis from the permanent magnets. There is greater variation in the quadrature axis synchronous reactance because the slope of the magnetisation curve is steeper in the q-axis operating region than in the d-axis region.

There is a difference in the direct axis static inductance levels between magnetising and demagnetising currents, caused by presaturation of the magnetic circuit by the permanent magnets. The operating point of the motor is shifted high up the linear region of the material saturation characteristic, so that the introduction of magnetising current will shift the operating point into saturation. A demagnetising current produces magnetic flux in opposition to that of the permanent magnets, shifting the operating point further down the linear region of the curve. Because the slope in the linear region is steeper than in the saturation region, the demagnetising synchronous reactance will be larger for a given current magnitude. The permanent magnets have no effect on the quadrature axis saturation levels. The synchronous reactance is the same for both magnetising and demagnetising current.

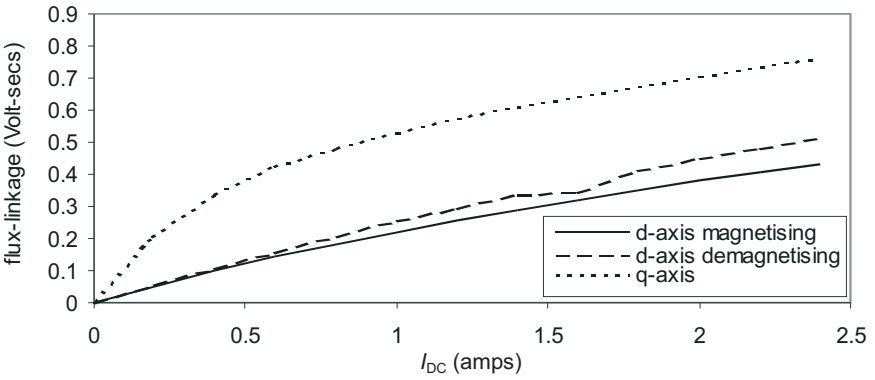

Fig. 4: Test motor 1 flux-linkages due to current

A number of papers discuss the pre-saturation of the magnetic circuit by the permanent magnets. [7] suggests that the direct axis flux-linkage will initially be the same for both magnetising and demagnetising currents. When the demagnetising current reaches a sufficient level to saturate the rotor bridge areas in the opposite direction, there will then be a step increase in flux-linkage, creating a difference between the magnetising and demagnetising flux-linkages that will remain as the current increases further. The explanation given in [7] is specific to the geometry of the rotor tested and the true nature of the synchronous reactances is, in fact, slightly different. The change between magnetising and demagnetising d-axis flux-linkage occurs as the saturation of the bridges is initially neutralised, not as it is reversed. The demagnetising current creates a flux in the rotor bridges that opposes the direction of the flux created by the permanent magnets. When the current is sufficiently high, these two components of flux will be of equal magnitude. At this point, both components of flux will flow across the airgap rather than through the bridges, resulting in the step change noted in [7, 8]. The step change results in an initial difference between the demagnetising and magnetising flux-linkages that will gradually decrease as the level of current is increased, due to saturation of the rotor bridges in the opposing direction.

This phenomenon is not immediately obvious from either the measure or simulated results of test motor 1, due to the construction of the rotor. The motor tested in [7] has solid rotor bridges; the slots are fully enclosed. In test motor 1, the slots are partially open. It is the difference in bridge permeability that affects the synchronous reactances. Whereas in the motor used in [7] bridge areas are saturated, the bridge areas in test motor 1 act as an extension of the airgap. Most flux

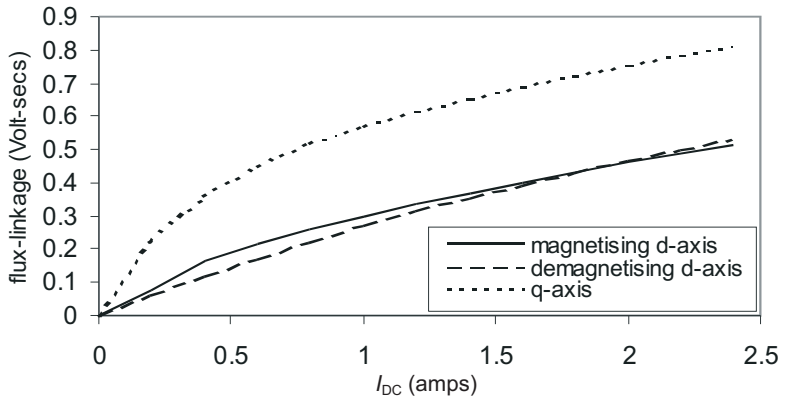

Fig. 5: Results of flux-linkage simulations for test motor 1 with remodelled rotor bridges

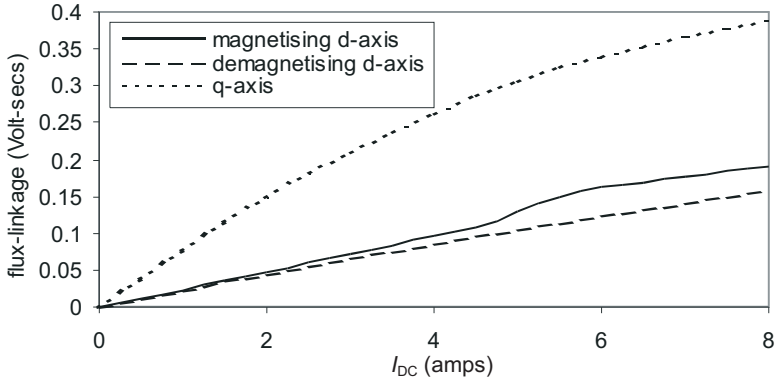

Fig. 6: Reliance motor with original geometry showing significant change in flux-linkage due to current

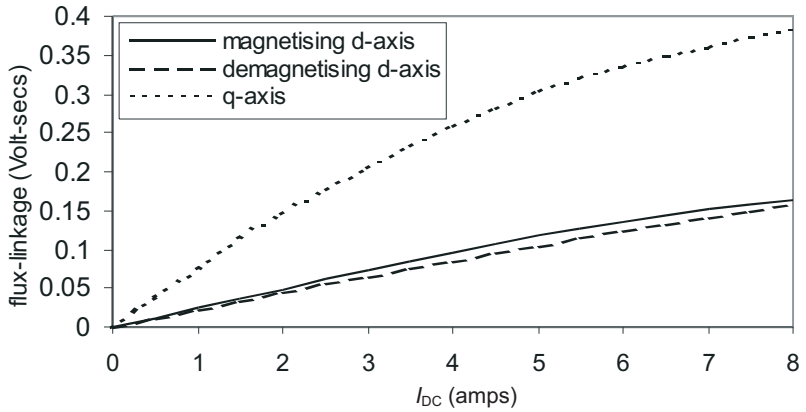

Fig. 7: Reliance motor with remodelled geometry showing no step change in flux-linkage due to current

flows across the airgap to the stator rather than between adjacent rotor bars and the difference in synchronous reactances is gradual rather than a step change. Test motor 1 was remodelled with the rotor bridges specified as the same material as the bars; the width of the bridges is such that there is a significant amount of leakage flux. The resulting flux-linkages are shown in Fig. 5. A second test motor, similar to that used in [7], has also been simulated. Fig. 6 shows the simulated values of flux-linkage due to current for the original geometry. When the bridges are removed to create open rotor slots, there is no longer a significant change in the flux-linkage, as shown in Fig. 7. The initial level of saturation in the bridges is decreased if the width is increased, thereby reducing the difference in flux-linkage levels for positive and negative currents.

5 Dependence of magnetisation characteristics on rotor bridge design

Fuller investigation into the effects of the rotor bridges has been carried out using the FE software. Test motor 1 has been modelled with four different bridge configurations: with the original open rotor slots (bridge areas are air) and with three different thicknesses of bridges with the same material as the rotor bars. Fig. 8 shows the results of synchronous reactance simulations for each configuration. Test motor 2 has been modelled with the original rotor design (rotor bridges are the same material as the rotor bars), with the bridges at half the

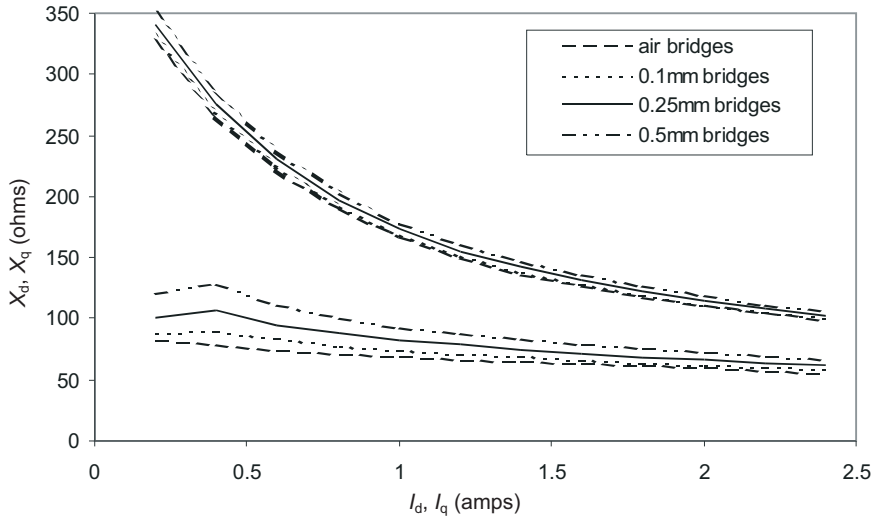

Fig. 8: Synchronous reactance simulation results for different bridge types (Test Motor 1)

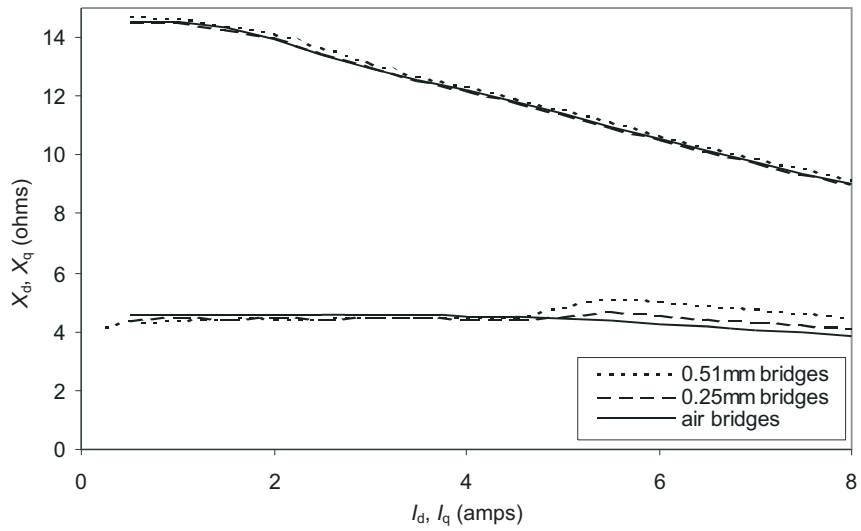

Fig. 9: Synchronous reactance simulation results for different bridge types (Test Motor 2)

Table 1: Comparison between partially open and fully closed rotor slots, showing significant increases in d-axis reactance and decreases in airgap flux density when bridge thickness is increased

Parameter	Test Motor 1			Test Motor 2	
	0.1 mm	0.25 mm	0.5 mm	0.25 mm	0.51 mm
X_q	+ 2 %	+ 4 %	+ 8 %	+ 0.7 %	+ 1.3 %
X_d	+ 14 %	+ 36 %	+ 63 %	+ 8 %	+ 19 %
Bgap (OC)	– 9 %	– 13 %	–17 %	– 2 %	– 4 %

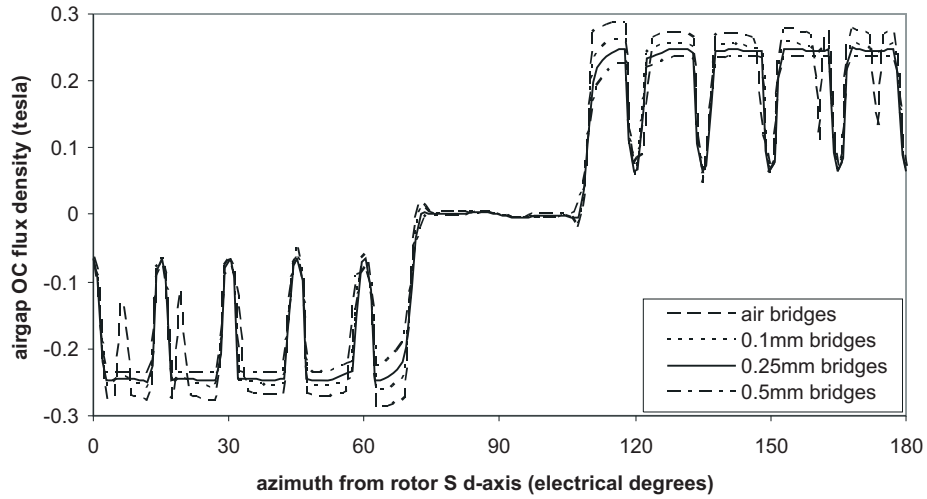

Fig. 10: Open circuit airgap flux density distribution of test motor

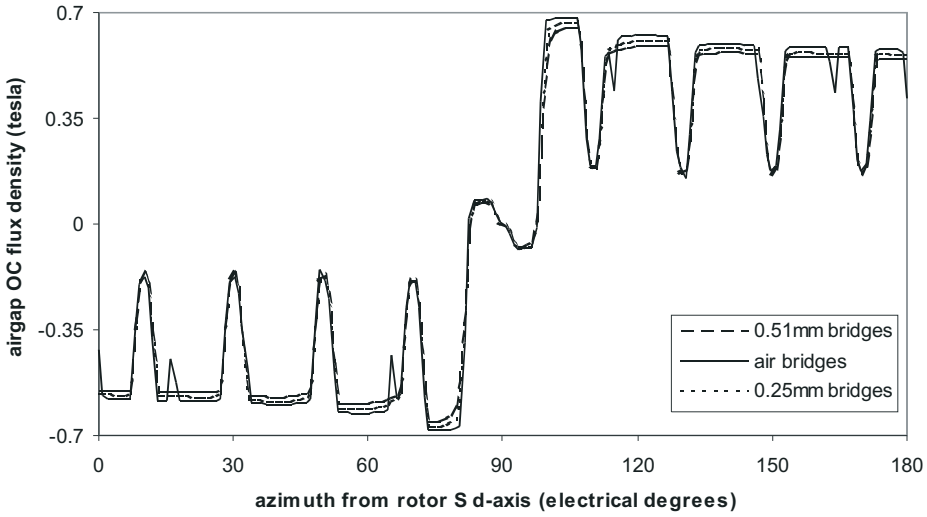

Fig. 11: Open circuit airgap flux density distribution of test motor 2

original thickness and with open rotor slots. The synchronous reactance simulation results are shown in Fig. 9.

The effect of the rotor bridges is to limit the levels of harmonics in the airgap flux density waveform. Figs. 10 and 11 show the open circuit airgap flux density distributions for test motors 1 and 2 respectively. For both test motors, the airgap flux density waveforms with highest harmonic content are those when the rotor slots are open. Introducing magnetic bridge sections to close the slots reduces the harmonic content of the waveforms, but also decreases the levels of airgap

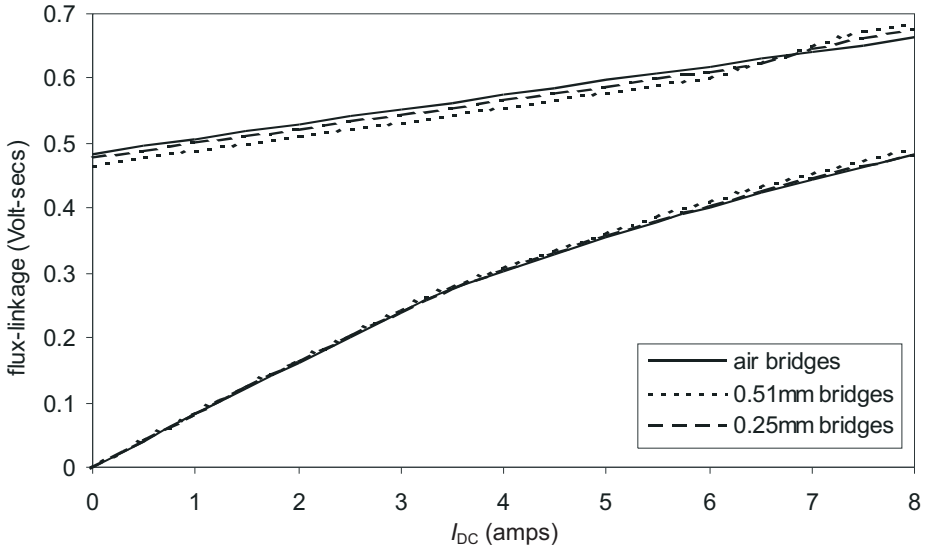

Fig. 12: Direct and quadrature axis magnetisation curves for one phase of test motor 2

flux density, as the bridges act as leakage paths for the flux. Increasing the thickness of these sections reduces the airgap flux density further, but does not make any discernible difference to the harmonic content of the flux density distribution. The simulation results are summarised in Table 1. It shows the maximum percentage changes in synchronous reactances and open circuit flux density waveforms, when open slots are remodelled with closed magnetic bridge sections of various thicknesses. The effects of adding the magnetic bridge sections are greater in the direct axis than the quadrature, because the rotor bars lying on the direct axis form a path for the magnet flux, whereas there is assumed to be no flux-linkage contribution from the magnet flux on the quadrature axis.

The effects of closing the rotor slots with magnetic bridge material can also been seen in the magnetisation curves of the test motors. At low current levels, the magnetic circuit is dominated by the flux contribution from the permanent magnets and so the total flux-linkage will be less for the rotor designs with magnetic bridges than for those with open slots. The degree to which the flux-linkage is reduced is dependent on the thickness of the bridges, but also on the rotor position. The quadrature axis magnetisation curve has no flux-linkage contribution from the magnet and so the difference will be minimal. On the direct axis the magnet contribution is greatest and so the difference in flux-linkage levels will be greatest. As the level of current increases, the difference in flux-linkage contributions from the current also increases. When the current reaches a certain level, the difference in flux-linkage will be greater than the difference in magnet flux crossing the airgap, and so the rotors with magnetic bridges will eventually produce more flux-linkage than those with open slots, as in Fig. 12.

6 Conclusions

The results from the finite element analysis show that the magnetisation characteristics of the permanent magnet motors are highly dependent on the rotor bridge design. The use of magnetic rotor bridges is advantageous in reducing harmonics in the flux density distribution and the addition of the bridge sections can lead to increases in flux-linkage at high current levels. However, designs incorporating closed rotor slots have been shown to increase leakage flux. A compromise must therefore be reached whereby the dimensions of the bridge sections reduce the harmonic levels in the flux density distribution and the leakage flux is kept to a reasonable level.

7 Acknowledgments

The authors acknowledge the support of the SPEED Consortium. J. A. Walker is funded by the UK Engineering and Physical Sciences Research Council, Robert Bosch GmbH and the SPEED Consortium. Thanks are given to Electrolux Compressors, for supply of test motors, to Jimmy Kelly and Wilson MacDougall for help with construction of the test rigs and to Dr. Mircea Popescu for many useful discussions.

References

[1] Miller, T. J. E., McGilp, M. I: *PC-FEA Version 3.0/5.0 User's Manual*. Glasgow: SPEED Laboratory, May 2002.

[2] IEEE Guide: *Test Procedures for Synchronous Machines*. IEEE Standard 115-1995 New York: Institute of Electrical and Electronic Engineers, Inc. 1995.

[3] Jones, C. V.: *The Unified Theory of Electrical Machines*. London: Butterworths, 1967.

[4] Prescott, J. C., El-Kharashi, A. K.: "A Method of Measuring Self-inductances Applicable to Large Electrical Machines." Proceedings of the Institution of Electrical Engineers **106** (Part A), 1959, p. 169–173.

[5] Miller, T. J. E.: *Switched Reluctance Motors and Their Control*. Oxford: Clarendon Press, 1993.

[6] Miller, T. J. E. et al.: "Calculating the Interior Permanent-Magnet Motor." Conference Record of the IEEE International Electric Machines and Drives Conference **2**, 2003, p. 1181–1187.

[7] Miller, T. J. E.: "Methods for Testing Permanent Magnet Polyphase AC Motors." Conference Record of the

IEEE Industry Applications Society Annual Meeting, 1981, p. 494–499.

[8] Rahman, M. A., Zhou, P.: "Analysis of Brushless Permanent Magnet Synchronous Motors." *IEEE Transactions on Industrial Electronics*. Vol. **43** (1996), p. 256–267.

Jill Alison Walker
e-mail: jwalker@elec.gla.ac.uk

Calum Cossar

T. J. E. Miller

SPEED Laboratory, University of Glasgow
Rankine Building
Oakfield Avenue
Glasgow G12 8LT, Scotland, UK

Appendix 1: Test motor parameters

Parameter	*Test motor 1*	*Test motor 2*
Stator lamination shape	Circular, chamfered edges	Circular
Stack length	39 mm	95.25 mm
Shaft radius	9.5 mm	15.75 mm
Rotor outer radius	31.72 mm	46.4 mm
Airgap length	0.28 mm	0.32 mm
Stator outer radius	64 mm	77.22 mm
Magnet thickness	5.8 mm	6.35 mm
No. of poles	2	4
No. of rotor bars	28	44
No. of stator slots	24	36
Rated voltage	220 V, 50 Hz	230 V, 60 Hz
Turns/ Phase	970	168
Winding configuration	Custom sine-distributed	Lap

